

Tukey-Inspired Video Object Segmentation

Brent A. Griffin Jason J. Corso
University of Michigan
{griffb, jjcorso}@umich.edu

Abstract

We investigate the problem of strictly unsupervised video object segmentation, *i.e.*, the separation of a primary object from background in video without a user-provided object mask or any training on an annotated dataset. We find foreground objects in low-level vision data using a John Tukey-inspired measure of “outlierness.” This Tukey-inspired measure also estimates the reliability of each data source as video characteristics change (*e.g.*, a camera starts moving). The proposed method achieves state-of-the-art results for strictly unsupervised video object segmentation on the challenging DAVIS dataset. Finally, we use a variant of the Tukey-inspired measure to combine the output of multiple segmentation methods, including those using supervision during training, runtime, or both. This collectively more robust method of segmentation improves the Jaccard measure of its constituent methods by as much as 28%.

1. Introduction

Video understanding remains a focus area in vision. Video object segmentation (VOS), a critical sub-problem, supports learning object class models [35, 45], scene parsing [28, 48], action recognition [30, 43, 44], and video editing applications [5]. Despite the utility of VOS, finding general solutions remains hotly in focus, especially in cases without human annotation or other supervision provided for training or inference. Most unsupervised methods make use of a measurable property, such as salient object motion [36], generic object appearance [11, 25], or rigid background elements [56]. However, a primary challenge in VOS is the variability of video characteristics: cameras can be static or moving; backgrounds and objects can be rigid or dynamic; objects can leave view, change scale, or become occluded; and unique elements like rippling water cause peculiar visual effects. In these circumstances, specific data sources become unreliable, degrading VOS performance.

We propose a new, strictly unsupervised VOS method called Tukey-Inspired Segmentation (TIS), which separates the primary foreground object in a video from background.



Figure 1. Tukey-inspired segmentation of DAVIS’s Parkour video, which has a moving camera, a dynamic foreground object with scale-variation, and occlusions (best viewed in color).

In *Exploratory Data Analysis* [53], John Tukey provides a statistical method to find outliers in data. Given that foreground objects typically exhibit a measurable difference relative to the surrounding background, we use Tukey’s statistical method to identify candidate foreground objects in low-level vision data. We also develop our own “outlierness” scale to quantitatively determine each data source’s ability to reveal foreground objects. By weighting and combining foreground candidates from multiple data sources, our output segmentation mitigates problems associated with changing video characteristics (see Figure 1). In addition, we use a variant of our “outlierness” scale to estimate the reliability of segmentations from multiple VOS frameworks, which we weight and combine to generate new, more reliable segmentations. Using our TIS method to find foreground objects in low-level vision data, we set a new precedent for unsupervised methods on the DAVIS benchmark dataset. Using our TIS variant to combine segmentations, we achieve better performance on DAVIS than all prior approaches, whether unsupervised or supervised.

2. Related Work

Learning-based methods have become commonplace for VOS benchmarks. However, supervised methods require annotated data, which are exceptionally tedious and costly for segmentation. For example, the state-of-the-art On-AVOS [54] has three distinct types of supervision: first, it trains its base network using the ImageNet [10], Microsoft COCO [27], and PASCAL datasets [12]; second, it fine-tunes using the DAVIS dataset [38]; and, third, it re-

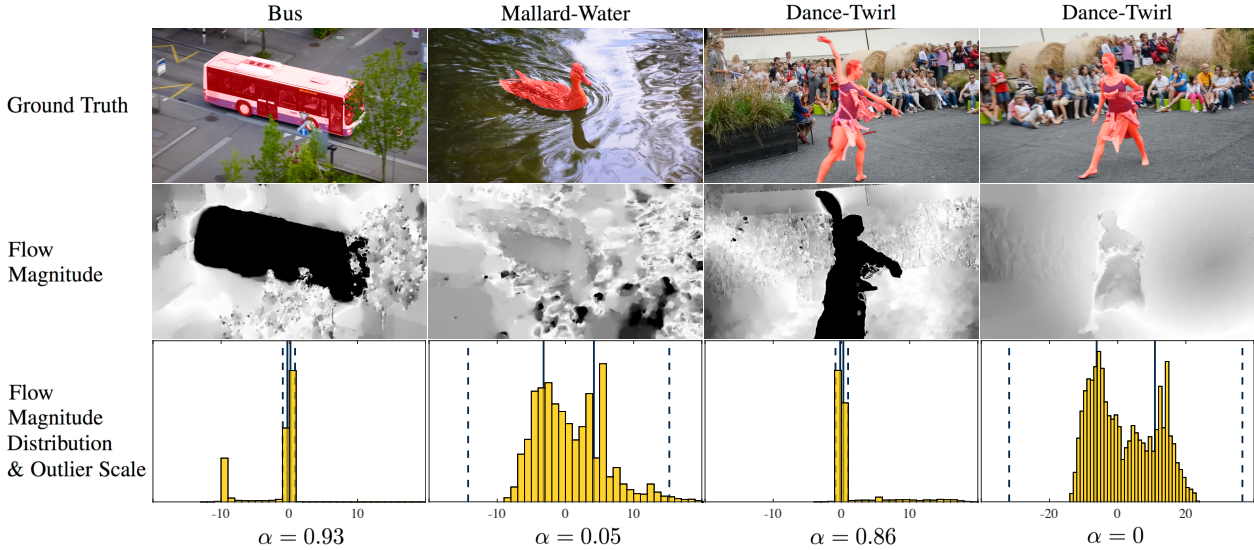


Figure 2. Foreground Candidates in Image Data. The outlier scale α acts as a saliency weighting that adapts to frame-to-frame video characteristics. In these examples, we focus on optical flow magnitude with outliers depicted as black pixels (middle row). Flow distributions are offset from the median (bottom row) and include the interquartile range (solid lines) and outlier thresholds (dotted lines). In the Bus video, the camera follows the bus while the background moves; from the resulting bimodal distribution, we reliably track the bus as a salient flow outlier ($\alpha = 0.93$). In Mallard-Water, due to dynamically flowing background elements, the mallard is difficult to track using flow magnitude ($\alpha = 0.05$). In Dance-Twirl, $\alpha = 0.86$ when the camera is relatively stationary and $\alpha = 0$ when the camera is moving.

quires a user-provided object mask at the beginning of each video. Other DAVIS benchmark leaders, such as OSVOS-S [31], RGMP [34], OSVOS [4], and MSK [37], have similar requirements. To support learning, some researchers develop their own weakly-annotated (FSEG [20]) or synthetic training data (LMP [49]). Other methods require supervision through components, such as features from a previously-trained network (OFL [52]) or a previously-trained boundary detection algorithm (ARP [24, 57]). Finally, some supervised algorithms are not trained, but still need a user-provided mask at runtime [1, 39, 15, 33]. In contrast, our TIS method has no labeling or training requirements. This design constraint supports application areas where user-provided masks are impractical and application-specific datasets for training are unavailable.

Multiple benchmarks are available to evaluate VOS methods [26, 51], including the Densely Annotated Video Segmentation (DAVIS) dataset [38]. DAVIS evaluates VOS methods across many challenge categories, including multiple instances of occlusions, objects leaving view, scale-variation, appearance change, edge ambiguity, camera-shake, interacting objects, and dynamic background (among others); these challenges frequently occur simultaneously. Using our strictly unsupervised TIS method, we achieve a Jaccard measure (or intersect over union) of 67.6 and, using the combinational variant, a Jaccard measure of 74.9, which is a 17% improvement over previous unsupervised results on DAVIS [3, 14, 16, 25, 36, 47, 55, 56].

Primary Contributions

Our primary contribution is a video object segmentation method that utilizes low-level processes without any training or annotation requirements, neither at training or runtime. Our method achieves the highest performance among all known unsupervised methods and higher performance than many supervised methods on the DAVIS video object segmentation benchmark for single objects, which is our focus. We also develop a variant of our initial approach that adaptively combines segmentations from multiple methods, generating new segmentations that achieve the highest DAVIS performance in every category of unsupervised and supervised approaches. We provide source code for the current work at www.github.com/griffbr/TIS.

3. Tukey-Inspired Segmentation

We derive two Tukey-inspired methods of segmentation. In Section 3.1, we find foreground objects directly from general image data. We identify foreground candidates using John Tukey’s statistical measure of outliers, then we use our own measure of “outlierness” to determine the reliability of each data source for identifying foreground objects. In Section 3.2, we combine a set of binary images that represent previous estimates of foreground object locations, which enables the simultaneous utilization of multiple segmentation methods. To improve accuracy, we use a second “outlierness” measure to determine the reliability of each source segmentation and weight its relative contribution.

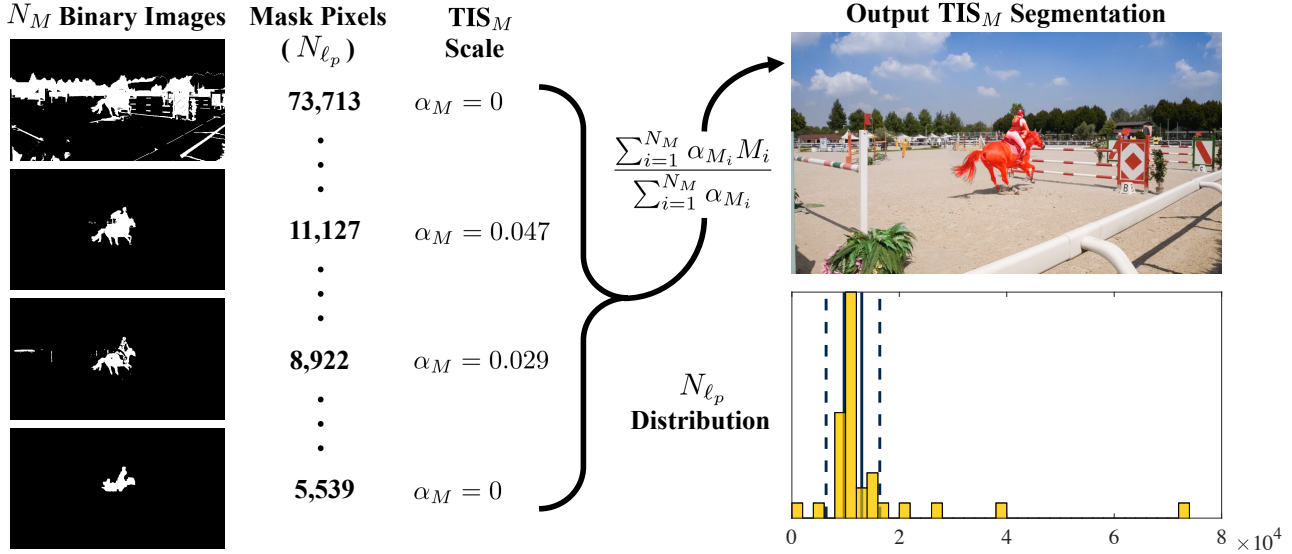


Figure 3. Foreground Objects from Binary Images. In this example, 34 segmentation methods are combined using the TIS_M method (i.e., $N_M = 34$). The binary image outlier scale α_M functions as a confidence weighting for each mask M and changes each video frame. Masks exhibiting a strong N_{ℓ_p} consensus with the group are considered reliable (middle left), while masks with too many or too few foreground pixels are considered unreliable outliers (top and bottom left, $\alpha_M = 0$). The N_{ℓ_p} distribution for the current video frame (bottom right) includes the interquartile range (solid lines) and outlier thresholds (dotted lines).

3.1. Foreground Candidates in Image Data

Most foreground objects exhibit a measurable difference in data relative to background elements. We identify this difference using outliers in vision data (e.g., optical flow). Given an image D containing data values $d_p \in \mathbb{R}$ for each pixel p , we calculate lower and upper outlier thresholds:

$$\begin{aligned} O_1 &= Q_1 - k(Q_3 - Q_1) \\ O_3 &= Q_3 + k(Q_3 - Q_1), \end{aligned} \quad (1)$$

where Q_1 and Q_3 are the lower and upper quartiles for all $d_p \in D$ and $Q_3 - Q_1$ is the interquartile range (Q_2 is the median). k is a constant that scales the outlier thresholds, O_1 and O_3 ; as suggested by John Tukey in [53], we use $k = 1.5$ to find “outliers.” We use each set of outlier data

$$O := \{d_p \in D | d_p < O_1 \vee d_p > O_3\} \quad (2)$$

to identify pixels corresponding to foreground objects.

We also define our own quantitative measure of “outlierness” for each data source D :

$$\alpha := \frac{\sum_{d_p \in O} |d_p|}{\sum_{d_p \in D} |d_p|}. \quad (3)$$

$\alpha \in [0, 1]$ is proportional to the magnitude of data in O relative to D . By calculating α for each data source, we approximate the frame-to-frame capacity of each source to track foreground objects in a variety of video settings (see Figure 2). Accordingly, we use α to weight each input data source for our example VOS implementation in Section 4.

3.2. Foreground Objects from Binary Images

As an alternative to finding foreground objects in image data, we derive a second outlier scale that enables us to combine segmentation masks from multiple methods and weight their relative contribution according to their frame-to-frame reliability (see Figure 3). Given a set of N_M binary masks for the same video frame, assume each mask M consists of pixel-level labels, $\ell_p \in \{0, 1\}$, where $\ell_p = 1$ indicates pixel p is a foreground-object location. Compared to image data, the “outlierness” of data within each M is relatively meaningless ($\ell_p \in \{0, 1\}$ implies that for $\ell_p \in M$: $Q_1, Q_2, Q_3 \in \{0, 1\}$). Instead, we measure “outlierness” across the set of binary images using the total number of foreground pixels in each M ,

$$N_{\ell_p} := \sum_{\ell_p \in M} \ell_p. \quad (4)$$

Using N_{ℓ_p} , the outlier scale for each mask is defined as

$$\alpha_M := \begin{cases} \max\left(\frac{N_{\ell_p} - O_1}{Q_2 - O_1}, 0\right) & \text{if } N_{\ell_p} < Q_2 \\ \max\left(\frac{N_{\ell_p} - O_3}{Q_2 - O_3}, 0\right) & \text{otherwise} \end{cases}, \quad (5)$$

where quartiles Q_1, Q_2 , and Q_3 and thresholds O_1 and O_3 are found using (1) on the set of N_{ℓ_p} from all N_M masks.

We use $\alpha_M \in [0, 1]$ to weight each mask based on proximity to the median number of foreground pixels across all N_M masks, with outliers being scaled at 0. The intuition behind this weighting is simple. If an individual mask is near

the median, it is representative of the collective consensus of segmentation masks for the approximate size of the foreground object, and it is likely more reliable. Alternatively, if an individual mask is an outlier, it is likely unreliable for the current video frame.

To generate the output segmentation mask, we define an image-level estimate of “foregroundness” as

$$F := \frac{\sum_{i=1}^{N_M} \alpha_{M_i} M_i}{\sum_{i=1}^{N_M} \alpha_{M_i}}, \quad (6)$$

where α_{M_i} is the outlier scale for the i th mask M_i . Note that F 's corresponding pixel-level values $f_p \in [0, 1]$. The final output mask M for the Tukey-inspired combination of binary images is found using

$$\ell_p = \begin{cases} 1 & \text{if } f_p > 0.5 \\ 0 & \text{otherwise} \end{cases}. \quad (7)$$

Remark: In Figure 3 and Section 5.2, we refer to this binary image-based segmentation method as TIS_M .

4. Tukey-Inspired Segmentation using Motion and Visual Saliency Outliers

We implement the method of finding foreground objects in image data from Section 3.1 using motion and visual saliency data. For motion saliency, x and y optical flow components are found using the method from [29]; in addition, the flow magnitude (i.e., $|x^2 + y^2|$) and flow angle (i.e., $\arctan(\frac{y}{x})$) are also calculated. For each flow measure, the outlier thresholds and scales are calculated on a frame-to-frame basis using (1)-(3). The pixel-level motion saliency measure, d_p^{ms} , is defined for each flow component as

$$d_p^{\text{ms}} := \begin{cases} 0 & \text{if } d_p \notin O \vee \alpha_f < 0.5 \\ \alpha_f |d_{p_f} - Q_{2_f}| & \text{otherwise} \end{cases}, \quad (8)$$

where d_{p_f} is the initial pixel-level flow component value with corresponding frame-to-frame median Q_{2_f} , outlier scale α_f , and a 0.5 minimum scale requirement.

The intuition behind (8) is as follows. First, whether a foreground object is moving with a fixed camera or vice versa, the foreground object's deviation from the frame's median optical flow will generally be salient (see Bus in Figure 2). Second, the absolute value enables a positive “foregroundness” contribution regardless of a flow component's sign. Finally, the minimum scale requirement will remove the influence of less reliable flow components.

We found that visual saliency is less useful than optical flow for most video segmentation cases. However, the product of visual saliency and optical flow is beneficial for videos with dynamic background elements (e.g., Mallard-Water in Figure 2). Thus, we include a pixel-level visual

saliency measure, d_p^{vs} , defined as

$$d_p^{\text{vs}} := (d_{p_v})^k \sum_{i=1}^4 \max(\alpha_{f_i}, 0.5) |d_{p_{f_i}} - Q_{2_{f_i}}|, \quad (9)$$

where $d_{p_v} \in [0, 1]$ is a pixel-level visual saliency-based scale (found using [32]), k is an exponential scale that adjusts the relative sharpness of $(d_{p_v})^k \in [0, 1]$, $d_{p_{f_i}}$ is the i th flow component with corresponding median $Q_{2_{f_i}}$ and outlier scale α_{f_i} , and the minimum applied scale of 0.5 ensures that visual saliency features are available even if $\alpha_{f_i} = 0 \forall i$. Three d_p^{vs} measures are used altogether, with $k = \{1, \frac{1}{2}, \frac{1}{3}\}$.

To generate the segmentation mask, we combine the four d_p^{ms} and three d_p^{vs} saliency measures for a pixel-level estimate of “foregroundness,” defined as

$$f_p := \sum_{i=1}^7 d_p^i, \quad (10)$$

where d_p^i is the i th measure. Using (10), we generate a mask M for each video frame with pixel-level labels

$$\ell_p = \begin{cases} 1 & \text{if } f_p > \beta \delta_p \\ 0 & \text{otherwise} \end{cases}, \quad (11)$$

where $\ell_p = 1$ indicates a foreground object and $\beta \in \mathbb{R}$ is the sum of the mean and standard deviation of f_p in the current frame. δ_p is the pixel-level previous-mask “discount”

$$\delta_p := \begin{cases} \frac{1}{2} & \text{if } \ell_{p,i-1} = 1 \\ 1 & \text{otherwise} \end{cases}. \quad (12)$$

In simple words, if f_p is greater than the pixel-level mean and standard deviation of “foregroundness” in the current frame, pixel p is considered a foreground object location. In addition, wherever p corresponds to a mask position in the previous frame, a half-threshold discount is applied, which encourages frame-to-frame continuity and gradually increasing accuracy of the segmentation mask. Finally, the output segmentation mask assumes a single foreground object hypothesis, so the mask in each frame is the single continuous segment with the greatest f_p sum.

Remark: In the remainder of the paper, we refer to this image data-based segmentation method as TIS_0 .

4.1. Consensus-based Boundary Refinement

To improve the boundary accuracy of (11), we use supervoxel consensus voting. This choice is motivated by previous VOS work in [14] that relates the “foregroundness” of superpixels to nearest neighbors across frames. Supervoxels, on the other hand, inherently exist across many frames and have shown promising results for relating features [46, 61] and detecting object boundaries [59]. Given a

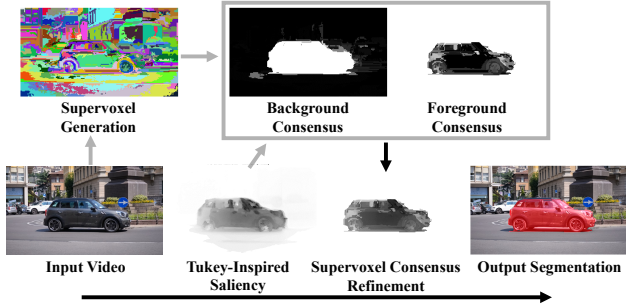


Figure 4. Consensus-based Boundary Refinement. Our Tukey-inspired segmentation (TIS_0) uses saliency outliers in image data to form a quantitative estimate of “foregroundness” and a corresponding object mask. Using supervoxels generated from the input video, we refine TIS_0 with a supervoxel-based consensus for both background and foreground elements, improving the boundary accuracy of the TIS_0 segmentation.

set of non-overlapping supervoxels that cover all video pixels, we use TIS_0 to build an internal consensus within the bounds of each supervoxel, and then relate this consensus across the video to refine the boundary of the initial TIS_0 mask. This refinement process is depicted in Figure 4.

First, using $\ell_p \in \{0, 1\}$ from (11), the local consensus within each supervoxel S is defined as

$$f_S^L := \frac{1}{N_p} \sum_{p \in S} (2\ell_p - 1), \quad (13)$$

where N_p is the number of pixels $p \in S$. Note that $f_S^L \in [-1, 1]$, where positive or negative values imply a foreground object or background.

Next, the non-local consensus among each S is found as

$$f_S^{NL} = \sum_{i=1}^{N_{NL}} w_i f_{S_i}^L, \quad (14)$$

where N_{NL} is the number of nearest-neighbors contributing to the non-local consensus for supervoxel S and w_i determines the relative weight of each neighbor. Because the total number of supervoxels, N_S , changes with each video, we set $N_{NL} = \lceil \frac{N_S}{100} \rceil$. Nearest neighbor weight w_i is set as

$$w_i = \frac{1}{R(S, S_i)^2}, \quad (15)$$

where $R \in \mathbb{R}$ calculates the city-block distance between the mean-LAB color of local supervoxel S and the i th nearest neighbor S_i . To ensure that all three LAB distances are meaningful, video-wide LAB values are linearly mapped between 0 and 1. R is squared to reduce the influence of supervoxels outside of the primary “clique.”

Finally, to refine the TIS_0 segmentation, we add (13) and (14) to the initial estimate of “foregroundness” from (10):

$$f'_p := f_p + w_0 f_S^L + f_S^{NL}, \quad (16)$$

Table 1. DAVIS Results for TIS_0 with and without Supervoxel Consensus Refinement. GBH-based refinement performs better when using only the local consensus. Higher numbers are better for rows labeled with \uparrow (e.g., \mathcal{J} mean) and worse for rows with \downarrow .

Configuration	Configuration ID		
	TIS_S	TIS_G^L	TIS_0
Supervoxels Used	SWA	GBH	None
Hierarchy Level	6	2	N/A
Local Consensus	Yes	Yes	N/A
Non-Local Consensus	Yes	No	N/A
Measure	DAVIS Results		
Region Similarity: \mathcal{J} Mean \uparrow	67.6	65.3	58.6
Contour Accuracy: \mathcal{F} Mean \uparrow	63.9	61.2	47.5
Temporal Stability: \mathcal{T} Mean \downarrow	31.0	31.8	30.7

where f_S^L are f_S^{NL} are the local and non-local consensus for the supervoxel containing p and w_0 determines the relative weight of f_S^L to f_S^{NL} . Essentially, f'_p improves the f_p -based boundary by adding to supervoxels with a consistent foreground object consensus while subtracting from supervoxels with a consistent background consensus. The refined TIS_0 segmentation mask is found using pixel-level labels

$$\ell_p = \begin{cases} 1 & \text{if } f'_p > 0 \\ 0 & \text{otherwise} \end{cases}. \quad (17)$$

Remarks: (a) f_p in (16) is scaled s.t. $f_p \in [0, 1]$. (b) If using only local consensus, $w_0 = 1$ in (16) and all non-local weights are zeroed. (c) If using local and non-local consensus, $w_0 = \frac{1}{3}$ and non-local weights are uniformly scaled s.t. $\sum_{i=1}^{N_{NL}} w_i = \frac{2}{3}$. (d) The refined mask (17) is limited to the two segments with the greatest f'_p sum in each frame. This improves VOS for objects with partial occlusions.

5. Results

We evaluate our TIS segmentation methods on two VOS benchmark datasets: the Densely Annotated Video Segmentation (DAVIS) dataset [38] and the Georgia Tech Segmentation and Tracking Dataset (SegTrackv2) [26, 51]. The DAVIS 2016 dataset includes 50 diverse videos, 30 training and 20 validation, all of which have ground truth annotations matching the single object hypothesis (unlike DAVIS 2017-18). The SegTrackv2 dataset has fewer videos than DAVIS, and only a subset match the single object hypothesis. SegTrackv2 also contains videos with different resolutions, which span from 76,800 to 230,400 pixels per frame.

Three standard benchmark measures evaluate the performance of our segmentation method: region similarity \mathcal{J} , contour accuracy \mathcal{F} , and temporal stability \mathcal{T} , which are all calculated using the definitions provided in [38]. Region similarity (also known as the intersect over union or Jaccard index [13]) provides an intuitive, scale-invariant evaluation

Table 2. **Complete DAVIS Results for State-of-the-Art Unsupervised Methods.** Methods are unsupervised, so we compare using both training and validation videos. Object recall measures the fraction of sequences scoring higher than 0.5, and decay quantifies the performance loss (or gain) over time [38]. TIS_0 exhibits the best decay performance; TIS_S and TIS_M achieve top results in all other categories.

Measure	Current Results			[56]							
	TIS_M	TIS_S	TIS_0	NLC	BGM	FST	KEY	MSG	CVOS	TRC	SAL
Mean \uparrow	74.9	67.6	58.6	64.1	62.5	57.5	56.9	54.3	51.4	50.1	42.6
\mathcal{J} Recall \uparrow	90.1	84.7	75.9	73.1	70.0	65.2	67.1	63.6	58.1	56.0	38.6
Decay \downarrow	5.8	4.0	2.3	8.6	-	4.4	7.5	2.8	12.7	5.0	8.4
Mean \uparrow	69.0	63.9	47.5	59.3	59.3	53.6	50.3	52.5	49.0	47.8	38.3
\mathcal{F} Recall \uparrow	83.8	78.5	48.8	65.8	66.2	57.9	53.4	61.3	57.8	51.9	26.4
Decay \downarrow	9.0	5.7	1.4	8.6	-	6.5	7.9	5.7	13.8	6.6	7.2

Table 3. **DAVIS Validation Set Results.** Runtime supervision requires a user-provided annotation frame for each segmentation video. Training supervision includes dataset training and dataset-trained components (e.g., OFL and ARP). The online benchmark distinguishes by runtime supervision only. TIS_0 -based methods achieve top unsupervised results; TIS_M -based methods achieve top results in all categories.

Measure	Supervision Required											Unsupervised					
	Runtime & Training							Runtime		Training							
	TIS_{M5}^V	TIS_M^{RTV}	OnAVOS	OSVOS-S	CINM	FAVOS	RGMP	TIS_M^{RV}	BVS	TIS_M^{TV}	PDB	ARP	TIS_M^V	TIS_S	TIS_0	FST	CUT
\mathcal{J} Mean	88.1	86.7	86.1	85.6	83.4	82.4	81.5	76.5	60.0	81.8	77.2	76.2	71.2	62.6	56.2	55.8	55.2
\mathcal{F} Mean	87.5	83.8	84.9	87.5	85.0	79.5	82.0	71.2	58.8	76.6	74.5	70.6	66.4	59.6	45.6	51.1	55.2

for the number of mislabeled foreground pixels with respect to a ground truth annotation. Given a foreground mask M and ground truth annotation G , $\mathcal{J} = \frac{M \cap G}{M \cup G}$. Contour accuracy evaluates the boundary of a segmentation by measuring differences between the closed set of contours for M and G . Finally, temporal stability is a measure based on the consistency of a mask between video frames.

5.1. TIS_0 Foreground Objects from Image Data

We evaluate our Tukey-inspired measure for finding foreground objects in image data using the TIS_0 implementation from Section 4. To improve boundary accuracy, we refine TIS_0 with supervoxel consensus (Section 4.1) using segmentation by weighted aggregation (SWA) [9, 40] and hierarchical graph-based (GBH) [18] supervoxels (both generated using the LIBSVX library [60]). Both TIS_0 refinement configurations are detailed in Table 1 with additional analysis provided in [17].

DAVIS results for TIS_0 -based methods are compared with state-of-the-art methods in Tables 2 and 3. TIS_0 exhibits the best decay performance for \mathcal{J} and \mathcal{F} and achieves a higher \mathcal{J} than all previous unsupervised methods on the DAVIS validation set. Multiple methods have better contour accuracy than TIS_0 , but the refinement process from Section 4.1 solves this problem. TIS_S , which improves TIS_0 with consensus-based boundary refinement, outperforms all unsupervised segmentation methods for both \mathcal{J} and \mathcal{F} .

SegTrackv2 results are provided in Table 4. We select videos from SegTrackv2 that use a single object hypothesis (like DAVIS). SegTrackv2 uses videos with different resolutions, causing individual hierarchy levels to have dramati-

cally different supervoxel quantities from one video to the next. Accordingly, we change supervoxel hierarchy levels for TIS_S and TIS_G^L between videos. Besides NLC and TIS_S , TIS_G^L achieves top results.

5.2. TIS_M Foreground Objects from Binary Images

We evaluate our Tukey-inspired measure for finding foreground objects in binary images (Section 3.2) by combining the segmentation methods listed in Table 5. Each combination set includes a certain level of supervision: strictly unsupervised (TIS_M), training on an annotated dataset (TIS_M^T), user-provided object mask at runtime (TIS_M^R), or both user-provided masks and dataset training (TIS_M^{RT}). Some source segmentation methods are only available on the DAVIS Validation Set; TIS_M configurations using these validation methods are only evaluated on the validation set and are distinguished by a V (e.g., TIS_M^V).

TIS_M -based methods achieve top DAVIS results for unsupervised segmentation and all categories of supervised segmentation, as shown in Table 3 and Figure 5. For the complete dataset, the relative \mathcal{J} increases over previous results in each category are: 17% for unsupervised (TIS_M to NLC), 6% for training (TIS_M^T to ARP), 18% for runtime (TIS_M^R to BVS), and 4% for runtime and training (TIS_M^{RT} to MSK). For the validation set, the relative increases are: 28% for unsupervised (TIS_M^V to FST), 6% for training (TIS_M^{TV} to PDB), 28% for runtime (TIS_M^{RV} to BVS), and 2% for runtime and training (TIS_{M5}^V to OnAVOS). The greatest increases for TIS_M combinations over constituent methods occur for categories with a lower \mathcal{J} score (see Figure 5).

To further evaluate TIS_M , we compare against two ad-

Table 4. **SegTrackv2** Results. Other results are directly from citation or comparative studies in [14, 20]. Videos are single-object only.

Video \mathcal{J} Mean	Unsupervised								Supervised	
	Current Results			[58]	[19]					
	TIS_G^L	TIS_S	TIS_0	NLC	ITS	HPF	KEY	FST	FSEG	HVS
Birdfall	62	54	23	74	73	58	49	18	38	57
Frog	78	50	61	83	80	58	0	54	57	67
Girl	69	70	65	91	86	69	88	55	67	32
Monkey	58	57	34	71	83	69	79	65	8	62
Parachute	88	88	67	94	96	94	96	76	52	69
Soldier	56	53	49	83	76	6	67	4	7	67
Worm	77	58	52	81	82	84	84	73	51	35
All	70	62	50	82	82	70	66	54	59	56

Table 5. DAVIS Results for Multiple TIS_M Configurations. Bold font indicates best performance for a given set of methods combined. With the exception of “Experimental Sets,” TIS_M configurations use all applicable methods from the online benchmark (davischallenge.org).

ID	Supervised	Configuration Methods Combined	Total	Results	
				\mathcal{J}	\mathcal{F}
Complete DAVIS Dataset					
TIS_M	No	TIS_S, TIS_0, FST [36], NLC[14], MSG[3], KEY[25], CVOS[47], TRC[16]	8	74.9	69.0
TIS_M^T	Training	TIS_M set + ARP[24], FSEG[20], LMP[49]	11	80.5	74.2
TIS_M^R	Runtime	TIS_M set + BVS[33], FCP[39], JMP[15], HVS[18], SEA[8]	13	78.2	73.5
TIS_M^{RT}	R. & T.	$TIS_M^R \cup TIS_M^T$ sets + MSK[37], CTN[22], VPN[21], OFL[52]	20	83.3	78.5
Baseline Comparisons on DAVIS Validation Set					
TIS_M^V	No	TIS_M set & CUT[23]	9	71.2	66.4
mean $_M$	No	“ ”	9	73.3	67.7
median $_M$	No	“ ”	9	64.8	60.0
TIS_M^{TV}	Training	$TIS_M^V \cup TIS_M^T$ sets + PDB[42], LVO[50], SFLU[8]	15	81.8	76.6
mean $_M$	Training	“ ”	15	80.8	75.3
median $_M$	Training	“ ”	15	76.0	70.3
TIS_M^{RV}	Runtime	$TIS_M^V \cup TIS_M^R$ sets	14	76.5	71.2
mean $_M$	Runtime	“ ”	14	76.7	70.8
median $_M$	Runtime	“ ”	14	70.3	64.4
TIS_M^{RTV}	R. & T.	$TIS_M^{RT} \cup TIS_M^{TV}$ sets + OSVOS-S[31], OnAVOS[54], CINM[2], PML[6], RGMP[34], FAVOS[7], OSVOS[4], SFLS[8], OSMN[62], PLM[41]	34	86.7	83.8
mean $_M$	R. & T.	“ ”	34	86.1	82.9
median $_M$	R. & T.	“ ”	34	80.6	77.1
Experimental Sets on DAVIS Validation Set					
TIS_{M5}^V	R. & T.	OSVOS-S, OnAVOS, CINM, RGMP, FAVOS	5	88.1	87.5
mean $_M$	R. & T.	“ ”	5	88.5	87.7
TIS_{M19}^V	R. & T.	TIS_{M5}^{RTV} and TIS_M^{RV} sets	19	85.8	82.6
mean $_M$	R. & T.	“ ”	19	83.8	80.4

ditional statistics-based methods for combining segmentations. First, we test a mean-based combination (mean $_M$) that averages all source masks together and outputs a foreground label where the pixel-level mean is higher than 0.5; this is equivalent to setting $\alpha_{M_i} = 1$ in (6). Second, we test a median-based combination (median $_M$) that outputs the source mask with the median number of foreground pixels (N_{ℓ_p} in (4)). For the baseline comparison in Table 5, TIS_M has the highest combined \mathcal{J} and \mathcal{F} score for all categories of supervision but one (mean $_M$ over TIS_M^V). In addition,

TIS_M is the only combination method that achieves higher \mathcal{J} scores than all source segmentation methods.

As a final experiment for combining segmentations, we additionally test a small set of the top-five methods (TIS_{M5}^V) and a larger set combining the same top-five methods with many poorer segmentations (TIS_{M19}^V). We postulate that the TIS_M combination method is well-suited for the larger, more variable set of segmentations, where the elimination of poorer-performing outliers and promotion of reliable inliers is critical. This is evidenced by TIS_{M19}^V and the other

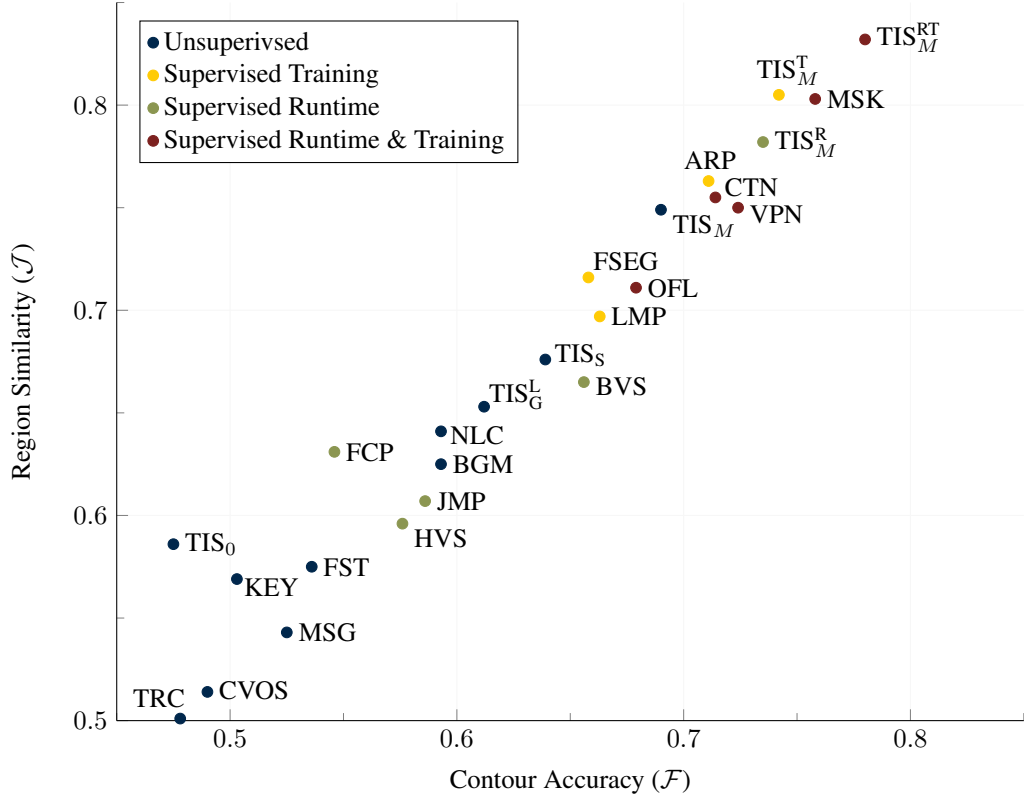


Figure 5. **Visual Comparison** of Segmentation Methods on **Complete DAVIS Dataset**. Note the correlation between \mathcal{J} and \mathcal{F} . The TIS_M segmentation methods improve performance across all categories of supervised and unsupervised methods.

large TIS_M sets in Table 5 outperforming $mean_M$. On the other hand, on a smaller, less variable set of segmentation methods, the calculation of quartiles and outliers for scaling is less meaningful; consequently, we find that the small-set TIS_{M5}^V and $mean_M$ have similar performance.

6. Discussion and Future Work

We develop a Tukey-inspired segmentation methodology to discover foreground objects in general image data. Our approach automatically adjusts its reliance on each data source according to the frame-to-frame characteristics of a video, addressing a primary challenge in video object segmentation of maintaining reliable measures with changing video characteristics. In addition, our Tukey-inspired measure for finding foreground objects in image data sets a new precedent on the DAVIS dataset for unsupervised segmentation methods. Our current implementation used optical flow and visual saliency data, but the method can incorporate additional sources of image data to accommodate new applications.

We apply a variant of our Tukey-inspired measure to combine the output of other segmentation methods, generating a new and collectively more robust method of segmentation. Our combination method achieves better per-

formance on the DAVIS dataset than all prior segmentation methods and represents a new paradigm in video object segmentation. In real-world applications, it is difficult to know which individual segmentation methods will perform best for various videos. On the other hand, by using our approach, multiple methods can be implemented simultaneously, and only the most reliable methods will be used for segmentation in any given video frame. This extension was particularly effective when constitute methods had variable performance and a large gap for improvement, indicating that the Tukey-inspired combination can be a viable tool for cutting-edge applications where performance has not yet reached its potential. Furthermore, we found that attempting to combine segmentations using “non-Tukey” methods can result in worse performance than some of the source segmentations. Finally, our combination method can easily incorporate new, better-performing segmentation methods as they are developed by the research community.

Given that the current results are restricted to a single object hypothesis, we are currently working on extending this approach to multiple objects. We are also exploring how our method of weighting input data based on “outlierness” can improve performance in supervised learning applications.

References

- [1] S. Avinash Ramakanth and R. Venkatesh Babu. Seamseg: Video object segmentation using patch seams. In *Proceedings of the IEEE Conference on Computer Vision and Pattern Recognition*, pages 376–383, 2014. 2
- [2] L. Bao, B. Wu, and W. Liu. CNN in MRF: video object segmentation via inference in A cnn-based higher-order spatiotemporal MRF. *CoRR*, abs/1803.09453, 2018. 7
- [3] T. Brox and J. Malik. Object segmentation by long term analysis of point trajectories. In *European conference on computer vision*, pages 282–295. Springer, 2010. 2, 7
- [4] S. Caelles, K.-K. Maninis, J. Pont-Tuset, L. Leal-Taixé, D. Cremers, and L. Van Gool. One-shot video object segmentation. In *Computer Vision and Pattern Recognition (CVPR)*, 2017. 2, 7
- [5] D.-J. Chen, H.-T. Chen, and L.-W. Chang. Video object cosegmentation. In *ACM International Conference on Multimedia*, 2012. 1
- [6] Y. Chen, J. Pont-Tuset, A. Montes, and L. Van Gool. Blazingly fast video object segmentation with pixel-wise metric learning. In *Computer Vision and Pattern Recognition (CVPR)*, 2018. 7
- [7] J. Cheng, Y.-H. Tsai, W.-C. Hung, S. Wang, and M.-H. Yang. Fast and accurate online video object segmentation via tracking parts. In *IEEE Conference on Computer Vision and Pattern Recognition (CVPR)*, 2018. 7
- [8] J. Cheng, Y.-H. Tsai, S. Wang, and M.-H. Yang. Segflow: Joint learning for video object segmentation and optical flow. In *IEEE International Conference on Computer Vision (ICCV)*, 2017. 7
- [9] J. J. Corso, E. Sharon, S. Dube, S. El-Saden, U. Sinha, and A. Yuille. Efficient multilevel brain tumor segmentation with integrated bayesian model classification. *IEEE transactions on medical imaging*, 27(5):629–640, 2008. 6
- [10] J. Deng, W. Dong, R. Socher, L. J. Li, K. Li, and L. Fei-Fei. Imagenet: A large-scale hierarchical image database. In *2009 IEEE Conference on Computer Vision and Pattern Recognition*, pages 248–255, June 2009. 1
- [11] I. Endres and D. Hoiem. *Category Independent Object Proposals*, pages 575–588. Springer Berlin Heidelberg, Berlin, Heidelberg, 2010. 1
- [12] M. Everingham, S. M. A. Eslami, L. Van Gool, C. K. I. Williams, J. Winn, and A. Zisserman. The pascal visual object classes challenge: A retrospective. *International Journal of Computer Vision*, 111(1):98–136, Jan 2015. 1
- [13] M. Everingham, L. Van Gool, C. K. Williams, J. Winn, and A. Zisserman. The pascal visual object classes (voc) challenge. *International journal of computer vision*, 88(2):303–338, 2010. 5
- [14] A. Faktor and M. Irani. Video segmentation by non-local consensus voting. In *BMVC*, volume 2, page 8, 2014. 2, 4, 7
- [15] Q. Fan, F. Zhong, D. Lischinski, D. Cohen-Or, and B. Chen. Jumpcut: non-successive mask transfer and interpolation for video cutout. *ACM Trans. Graph.*, 34(6):195, 2015. 2, 7
- [16] K. Fragkiadaki, G. Zhang, and J. Shi. Video segmentation by tracing discontinuities in a trajectory embedding. In *Computer Vision and Pattern Recognition (CVPR)*, 2012 *IEEE Conference on*, pages 1846–1853. IEEE, 2012. 2, 7
- [17] B. A. Griffin and J. J. Corso. Video object segmentation using supervoxel-based gerrymandering. *CoRR*, abs/1704.05165, 2017. 6
- [18] M. Grundmann, V. Kwatra, M. Han, and I. Essa. Efficient hierarchical graph-based video segmentation. In *2010 IEEE Computer Society Conference on Computer Vision and Pattern Recognition*, pages 2141–2148, June 2010. 6, 7
- [19] E. Haller and M. Leordeanu. Unsupervised object segmentation in video by efficient selection of highly probable positive features. In *2017 IEEE International Conference on Computer Vision (ICCV)*, pages 5095–5103, Oct 2017. 7
- [20] S. D. Jain, B. Xiong, and K. Grauman. Fusionseg: Learning to combine motion and appearance for fully automatic segmentation of generic objects in videos. *arXiv preprint arXiv:1701.05384*, 2017. 2, 7
- [21] V. Jampani, R. Gadde, and P. V. Gehler. Video propagation networks. In *2017 IEEE Conference on Computer Vision and Pattern Recognition (CVPR)*, pages 3154–3164, July 2017. 7
- [22] W. D. Jang and C. S. Kim. Online video object segmentation via convolutional trident network. In *2017 IEEE Conference on Computer Vision and Pattern Recognition (CVPR)*, pages 7474–7483, July 2017. 7
- [23] M. Keuper, B. Andres, and T. Brox. Motion trajectory segmentation via minimum cost multicuts. In *IEEE International Conference on Computer Vision (ICCV)*, 2015. 7
- [24] Y. J. Koh and C. S. Kim. Primary object segmentation in videos based on region augmentation and reduction. In *2017 IEEE Conference on Computer Vision and Pattern Recognition (CVPR)*, pages 7417–7425, July 2017. 2, 7
- [25] Y. J. Lee, J. Kim, and K. Grauman. Key-segments for video object segmentation. In *Computer Vision (ICCV)*, 2011 *IEEE International Conference on*, pages 1995–2002. IEEE, 2011. 1, 2, 7
- [26] F. Li, T. Kim, A. Humayun, D. Tsai, and J. M. Rehg. Video segmentation by tracking many figure-ground segments. In *The IEEE International Conference on Computer Vision (ICCV)*, December 2013. 2, 5
- [27] T.-Y. Lin, M. Maire, S. Belongie, J. Hays, P. Perona, D. Ramanan, P. Dollár, and C. L. Zitnick. Microsoft coco: Common objects in context. In D. Fleet, T. Pajdla, B. Schiele, and T. Tuytelaars, editors, *Computer Vision – ECCV 2014*, pages 740–755, Cham, 2014. Springer International Publishing. 1
- [28] B. Liu and X. He. Multiclass semantic video segmentation with object-level active inference. In *IEEE Conference on Computer Vision and Pattern Recognition*, 2015. 1
- [29] C. Liu. *Beyond pixels: exploring new representations and applications for motion analysis*. PhD thesis, Citeseer, 2009. 4
- [30] J. Lu, R. Xu, and J. J. Corso. Human action segmentation with hierarchical supervoxel consistency. In *IEEE Conference on Computer Vision and Pattern Recognition*, 2015. 1
- [31] K. Maninis, S. Caelles, Y. Chen, J. Pont-Tuset, L. Leal-Taixé, D. Cremers, and L. V. Gool. Video object segmentation without temporal information. *IEEE Transactions on Pattern Analysis and Machine Intelligence*, pages 1–1, 2018. 2, 7

- [32] R. Margolin, A. Tal, and L. Zelnik-Manor. What makes a patch distinct? In *Proceedings of the IEEE Conference on Computer Vision and Pattern Recognition*, pages 1139–1146, 2013. 4
- [33] N. Mrki, F. Perazzi, O. Wang, and A. Sorkine-Hornung. Bilateral space video segmentation. In *2016 IEEE Conference on Computer Vision and Pattern Recognition (CVPR)*, pages 743–751, June 2016. 2, 7
- [34] S. W. Oh, J.-Y. Lee, K. Sunkavalli, and S. J. Kim. Fast video object segmentation by reference-guided mask propagation. In *The IEEE Conference on Computer Vision and Pattern Recognition (CVPR)*, 2018. 2, 7
- [35] D. Oneata, J. Revaud, J. Verbeek, and C. Schmid. Spatio-temporal object detection proposals. In *European Conference on Computer Vision*, 2014. 1
- [36] A. Papazoglou and V. Ferrari. Fast object segmentation in unconstrained video. In *Proceedings of the IEEE International Conference on Computer Vision*, pages 1777–1784, 2013. 1, 2, 7
- [37] F. Perazzi, A. Khoreva, R. Benenson, B. Schiele, and A. Sorkine-Hornung. Learning video object segmentation from static images. In *Computer Vision and Pattern Recognition*, 2017. 2, 7
- [38] F. Perazzi, J. Pont-Tuset, B. McWilliams, L. Van Gool, M. Gross, and A. Sorkine-Hornung. A benchmark dataset and evaluation methodology for video object segmentation. In *Proceedings of the IEEE Conference on Computer Vision and Pattern Recognition*, pages 724–732, 2016. 1, 2, 5, 6
- [39] F. Perazzi, O. Wang, M. Gross, and A. Sorkine-Hornung. Fully connected object proposals for video segmentation. In *Proceedings of the IEEE International Conference on Computer Vision*, pages 3227–3234, 2015. 2, 7
- [40] E. Sharon, M. Galun, D. Sharon, R. Basri, and A. Brandt. Hierarchy and adaptivity in segmenting visual scenes. *Nature*, 442(7104):810–813, 2006. 6
- [41] J. Shin Yoon, F. Rameau, J. Kim, S. Lee, S. Shin, and I. So Kweon. Pixel-level matching for video object segmentation using convolutional neural networks. In *The IEEE International Conference on Computer Vision (ICCV)*, Oct 2017. 7
- [42] H. Song, W. Wang, S. Zhao, J. Shen, and K.-M. Lam. Dilated pyramid convolution and deeper bidirectional convlstm for video salient object detection. In *The European Conference on Computer Vision (ECCV)*, September 2018. 7
- [43] K. Soomro, H. Idrees, and M. Shah. Action localization in videos through context walk. In *IEEE International Conference on Computer Vision*, 2015. 1
- [44] K. Soomro, H. Idrees, and M. Shah. Predicting the where and what of actors and actions through online action localization. In *IEEE Conference on Computer Vision and Pattern Recognition*, 2016. 1
- [45] K. Tang, R. Sukthankar, J. Yagnik, and L. Fei-Fei. Discriminative segment annotation in weakly labeled video. In *IEEE Conference on Computer Vision and Pattern Recognition*, 2013. 1
- [46] E. H. Taralova, F. De la Torre, and M. Hebert. Motion words for videos. In *European Conference on Computer Vision*, pages 725–740. Springer, 2014. 4
- [47] B. Taylor, V. Karasev, and S. Soatto. Causal video object segmentation from persistence of occlusions. In *Proceedings of the IEEE Conference on Computer Vision and Pattern Recognition*, pages 4268–4276, 2015. 2, 7
- [48] J. Tighe and S. Lazebnik. Superparsing: scalable nonparametric image parsing with superpixels. *International Journal of Computer Vision*, 2012. 1
- [49] P. Tokmakov, K. Alahari, and C. Schmid. Learning motion patterns in videos. In *2017 IEEE Conference on Computer Vision and Pattern Recognition (CVPR)*, pages 531–539, July 2017. 2, 7
- [50] P. Tokmakov, K. Alahari, and C. Schmid. Learning video object segmentation with visual memory. In *2017 IEEE International Conference on Computer Vision (ICCV)*, pages 4491–4500, Oct 2017. 7
- [51] D. Tsai, M. Flagg, A. Nakazawa, and J. M. Rehg. Motion coherent tracking using multi-label mrf optimization. *International journal of computer vision*, 100(2):190–202, 2012. 2, 5
- [52] Y. H. Tsai, M. H. Yang, and M. J. Black. Video segmentation via object flow. In *2016 IEEE Conference on Computer Vision and Pattern Recognition (CVPR)*, pages 3899–3908, June 2016. 2, 7
- [53] J. W. Tukey. Exploratory data analysis. 1977. 1, 3
- [54] P. Voigtlaender and B. Leibe. Online adaptation of convolutional neural networks for video object segmentation. In *BMVC*, 2017. 1, 7
- [55] W. Wang, J. Shen, and F. Porikli. Saliency-aware geodesic video object segmentation. In *Proceedings of the IEEE Conference on Computer Vision and Pattern Recognition*, pages 3395–3402, 2015. 2
- [56] S. Wehrwein and R. Szeliski. Video segmentation with background motion models. In *British Machine Vision Conference*, 2017. 1, 2, 6
- [57] P. Weinzaepfel, J. Revaud, Z. Harchaoui, and C. Schmid. Learning to detect motion boundaries. In *2015 IEEE Conference on Computer Vision and Pattern Recognition (CVPR)*, pages 2578–2586, June 2015. 2
- [58] F. Xiao and Y. J. Lee. Track and segment: An iterative unsupervised approach for video object proposals. In *2016 IEEE Conference on Computer Vision and Pattern Recognition (CVPR)*, pages 933–942, June 2016. 7
- [59] C. Xu and J. J. Corso. Evaluation of super-voxel methods for early video processing. In *Computer Vision and Pattern Recognition (CVPR)*, 2012 IEEE Conference on, pages 1202–1209. IEEE, 2012. 4
- [60] C. Xu and J. J. Corso. Libsvx: A supervoxel library and benchmark for early video processing. *International Journal of Computer Vision*, 119(3):272–290, 2016. 6
- [61] C. Xu, S. Whitt, and J. J. Corso. Flattening supervoxel hierarchies by the uniform entropy slice. In *The IEEE International Conference on Computer Vision (ICCV)*, December 2013. 4
- [62] L. Yang, Y. Wang, X. Xiong, J. Yang, and A. K. Katsaggelos. Efficient video object segmentation via network modulation. *CVPR*, 2018. 7